References

1. Smith CJ, Olsen CH, Mocroft A, *et al.* **The role of antiretroviral therapy in the incidence of pancreatitis in HIV-positive individuals in the EuroSIDA study.** *AIDS* 2008; **22**: 47–56.
2. Fessel J, Hurley LB. **Incidence of pancreatitis in HIV-infected patients: comment on findings from in EuroSIDA cohort.** *AIDS* 2008; **22**:145–147.
3. Maxson CJ, Greenfield SM, Turner JL. **Acute pancreatitis as a common complication of 2′,3′-dideoxyinosine therapy in the acquired immunodeficiency syndrome.** *Am J Gastroenterol* 1992; **87**:708–713.
4. Moore RD, Keruly JC, Chaisson RE. **Incidence of pancreatitis in HIV-infected patients receiving nucleoside reverse transcriptase inhibitor drugs.** *AIDS* 2001; **15**:617–620.
5. Smith CJ, Mocroft A, Olsen CH, *et al. Incidence of pancreatitis amongst HIV-positive individuals, and the association with triglycerides and antiretroviral use [Abstract number P9.10/02].* In: 11th European AIDS Conference, 24–27 October, Madrid, Spain; 2007.

Immune reconstitution syndrome to *Strongyloides stercoralis* infection

We thank McCarthy and Currie for their response [1] to our case report [2], which described a young Eritrean man with HIV and hepatitis B infections who presented with an inflammatory colitis, 6 weeks after starting antiretroviral therapy and had *Strongyloides* larvae detected in stool samples. After treatment with ivermectin, his symptoms, and the associated intestinal dilatation, resolved. His presentation was localized to the intestines and comprised loss of appetite, abdominal pain, vomiting and weight loss. There were no respiratory symptoms and no evidence of dissemination of *Strongyloides* larvae or bacterial sepsis.

We have seen and recognized the well established, strong association of corticosteroid treatment with *Strongyloides* hyperinfection syndrome [3–5] and agree that excluding *Strongyloides* infection is important when considering steroid treatment in individuals who have lived in an endemic area [1]. We also concur that immune suppression due to HIV infection itself does not appear to cause hyperinfection [6]. In this case, however, although this patient had received steroid treatment (for thrombocytopaenia) in the weeks preceding presentation, there was no evidence of dissemination of the parasite outside the gastrointestinal system, and therefore a local inflammatory response, coinciding with rapid immunological recovery due to antiretroviral treatment, fits much better with the clinical picture. We, therefore, proposed that this case comprises immune reconstitution syndrome and not disseminated infection secondary to corticosteroid therapy.

Acknowledgement

There is no conflict of interests.

Clare L. Taylor and Andrew P. Ustianowski, *Monsall Unit, Department of Infectious Diseases and Tropical Medicine, North Manchester General Hospital, Delaunarys Road, Crumpsall, Manchester, UK.*

References

1. McCarthy JS, Currie B. **Immune reconstitution syndrome to *Strongyloides stercoralis* infection: authors' response.** *AIDS* 2007; **21**:1985–1986.
2. Taylor CL, Subbarao V, Gayed S, Ustianowski AP. **Immune reconstitution syndrome to *Strongyloides stercoralis* infection.** *AIDS* 2007; **21**:649–650.
3. Davidson RA, Fletcher RH, Chapman LE. **Risk factors for strongyloidiasis: a case control study.** *Arch Intern Med* 1984; **144**: 321–324.
4. Asdamongkol N, Pornsuriyasak P, Sungkanuparph S. **Risk factors for *Strongyloides* hyperinfection and clinical outcomes.** *Southeast Asian J Trop Med Public Health* 2006; **27**:875–885.
5. Ghosh K, Ghosh K. ***Strongyloides stercoralis* septicaemia following steroid therapy for eosinophilia: report of three cases.** *Trans R Soc Trop Med Hyg* 2007; **101**:1163–1165.
6. Viney ME, Brown M, Omoding NE, Bailey JW, Gardner MP, Roberts E, *et al.* **Why does HIV infection not lead to disseminated strongyloidiasis?** *J Infect Dis* 2004; **190**:2175–2180.

Protein Engineering, Design & Selection vol. 21 no. 10 pp. 597–603, 2008
Published online July 11, 2008 doi:10.1093/protein/gzn037

Preferential heterodimerization of a bispecific diabody based on a humanized anti-EGFR antibody 528

Ryutaro Asano[1], Yukiko Sone[1], Keiko Ikoma[1], Hiroki Hayashi[2], Takeshi Nakanishi[1], Mitsuo Umetsu[1], Yu Katayose[2], Michiaki Unno[2], Toshio Kudo[3] and Izumi Kumagai[1,4]

[1]Department of Biomolecular Engineering, Graduate School of Engineering, Tohoku University, Sendai 980-8579, [2]Division of Gastroenterological Surgery, Department of Surgery, Graduate School of Medicine, Tohoku University, Sendai 980-8574 and [3]Cell Resource Center for Biomedical Research, Institute of Development, Aging, and Cancer, Tohoku University, Sendai 980-8575, Japan

[4]To whom correspondence should be addressed.
E-mail: kmiz@kuma.che.tohoku.ac.jp

We report the utility of *in vitro* refolding in the preparation of monomorphous hEx3 bispecific diabodies with epidermal growth factor receptor and CD3 retargeting from insoluble aggregates in *Escherichia coli*. Appropriate interaction between cognate variable heavy and light chains led to the formation of functional hEx3 heterodimers in a diabody format rather than inactive homodimers. The refolded hEx3 was found to exhibit almost the equivalent activity to the hEx3 and single-chain hEx3 (hEx3-scDb) prepared in a mammalian secretion system. We suggest that the preparation of hEx3 from bacterial insoluble material by means of *in vitro* refolding would be useful for industrial-scale production of the diabody for its potential use in clinical studies.

Keywords: bispecific diabody/cancer immunotherapy/EGFR/*in vitro* refolding/small recombinant antibody

Introduction

Bispecific antibodies (BsAbs) are recombinant antibodies that can bind to two different epitopes on antigens. Bispecificity can be used in cancer immunotherapy to crosslink tumor cells to immune cells such as cytotoxic T cells, natural killer cells and macrophages. This crosslinking accelerates the destruction of the tumor cells by the immune cells, so that the high potency of BsAb may translate into improved antitumor therapy and lower costs of production because of the smaller doses needed (Cao *et al.*, 2003; Kufer *et al.*, 2004). However, the use of BsAbs in clinical studies has been hampered by difficulties in their large-scale production. Conventional chemical conjugation has been used, but the quality of the antibody produced is inconsistent (Raso *et al.*, 1981). The production of BsAbs by somatic fusion of two hybridomas to form a quadroma yields BsAbs of more consistent quality but involves the formation of various chain-shuffled antibodies; for instance, 10 different antibodies can be generated after random association of two heavy and two light chains (Suresh *et al.*, 1986; Kriangkum *et al.*, 2001).

Advances in recombinant technology have made it feasible to generate small recombinant BsAbs constructed from two different variable antibody fragments; these recombinant BsAbs include minibodies (Shahied *et al.*, 2004), tandem single-chain Fvs (scFvs) (Schlereth *et al.*, 2005) and diabodies (Arndt *et al.*, 1999). Compared with classic BsAbs prepared through chemical conjugation or quadroma production, compounds such as diabodies are smaller (approximately 55 kDa), thus facilitating rapid tissue penetration, high target retention and rapid blood clearance (Sundaresan *et al.*, 2003; Holliger *et al.*, 2005; Robinson *et al.*, 2005). Although downsizing BsAbs enables their large-scale preparation through bacterial expression systems, efficient overexpression of small functional BsAbs has not yet been achieved because the expression products form insoluble aggregates in the cytoplasmic or periplasmic space (Helfrich *et al.*, 1998; Tsumoto *et al.*, 1998; Arndt *et al.*, 1999; Peipp *et al.*, 2002).

We previously reported a system for preparing functional soluble scFvs from insoluble aggregates by means of an *in vitro* refolding system, and the same protocol could be applied for refolding heterodimeric proteins, including Fv (Takemura *et al.*, 2000, 2002; Asano *et al.*, 2002b). One of the previously generated diabodies, designated Ex3, retargets lymphokine-activated killer cells with the T-cell phenotype (T-LAK cells) against epidermal growth factor-positive (EGFR-positive) cell lines and shows remarkable antitumor activity *in vitro* and *in vivo* (Hayashi *et al.*, 2004). We also successfully produced a humanized Ex3 (designated hEx3) which had the same level of biological activity as Ex3 (Asano *et al.*, 2006).

The *in vitro* refolding system is promising for large-scale preparation of functional diabodies. However, that the refolded dimeric fraction contains inactive conformations of homodimers, which are formed from only one chain of the two elements in a bispecific diabody, has remained a concern because the nearly equivalent molecular weights of the homodimer and heterodimer complicates their separation. Here we analyzed the characteristics of the interaction between the hetero scFv fragments (hOHh5L and h5HhOL) used to construct hEx3 diabodies by gel filtration chromatography. We also compared the biological activities of the refolded hEx3 fractions and those produced by secretion from mammalian cells. The hetero scFv fragments accurately formed functional heterodimeric hEx3 diabodies with little non-functional homodimer. We show that interaction between cognate variable heavy (VH) and light (VL) domains yielded homomorphous hEx3 diabodies through both our refolding protocol and the secretory expression system.

Materials and methods

Expression of recombinant BsAbs

The hEx3 bispecific diabody was constructed from variable regions of the humanized anti-EGFR antibody 528 and anti-CD3 antibody OKT3 and the procedure for the construction of expression vectors and preparation of hEx3 has been

reported previously (Asano *et al.*, 2006). In brief, *Escherichia coli* strain BL21 (DE3) harboring a bacterial expression vector (pRA-hOHh5L for hOHh5L and pRA-h5HhOL for h5HhOL) was grown at 28°C in Luria–Bertani broth. After induction of protein production with isopropyl β-D-1-thiogalactopyranoside, cells were harvested by centrifugation (2000×*g*, 35 min), resuspended in 10 ml phosphate-buffered saline (PBS), ultrasonicated at 150 W for 15 min and centrifuged at 4500×*g* for 20 min. The resulting separated intracellular insoluble fraction was solubilized overnight at 4°C in 10 ml of 6 M guanidinium hydrochloride (Gu-HCl) in PBS. Solubilized proteins were purified through a TALON Metal Affinity Resin column (Clontech, Palo Alto, CA, USA).

Refolding of BsAbs

We applied two methods to prepare hEx3 diabodies from the purified hetero-scFv fragments hOHh5L and h5HhOL. In refolding process I, each of the hOHh5L and h5HhOL scFv solutions was diluted to 15 μM with 6 M Gu-HCl in PBS, and then the resulting solutions were mixed at a 1:1 ratio. The denatured scFv mixture solution (5 ml) underwent stepwise dialysis into PBS through solutions of 3, 2, 1 and 0.5 M Gu-HCl in PBS (Asano *et al.*, 2006). In process II, solutions of hOHh5L and h5HhOL scFv solutions were refolded individually by stepwise dialysis, and then the solutions were mixed at a 1:1 ratio.

Preparation of secreted BsAbs

To prepare secreted hEx3 and hEx3-scDb, Chinese hamster ovary (CHO) cells were transfected with the mammalian expression vector pcDNA-hEx3-scDb (for hEx3-scDb) or co-transfected with equal amounts of DNA of vectors pcDNA-hOHh5L and pcDNA-h5HhOL (for hEx3). A CHO clone that stably expressed each BsAb was established after screening with a selection medium containing an antibiotic [500 μg/ml G418 (Nacalai Tesque, Kyoto, Japan; for hEx3-scDb) and plus 200 μg/ml hygromycin (InvivoGen, San Diego, CA, USA; for hEx3)]. The cells were incubated in selection medium for 3 days at 37°C by roller-bottle culture and then switched to serum-free medium. The supernatant was collected after 4 days, and BsAbs were purified through a TALON Metal Affinity Resin column (Clontech). The buffer in the fractions containing antibodies was exchanged for PBS by dialysis, and the antibodies were concentrated with Centriprep 10 concentrators (Millipore, Tokyo, Japan). Finally, the concentrated samples were filtered through 0.22 μm ultrafiltration membrane (Millipore) and stored in PBS at 4°C (Asano *et al.*, 2007).

Gel filtration chromatography

Gel filtration analysis with a Hiload Superdex 200-pg column (10/300; GE Healthcare Bio-Science Corp., Piscataway, NJ, USA) was used to evaluate the structure of the dimer or monomer. The column was equilibrated with PBS, and then 250 μl of purified recombinant antibodies was applied to the column at a flow rate of 0.5 ml/min. To evaluate long-term stability, the secreted hEx3 peak corresponding to the dimer molecular weight was collected and then reanalyzed under the same conditions after storage for 6 months at 4°C.

Preparation of PBMCs and T-LAK cells

Peripheral blood mononuclear cells (PBMCs) were isolated by density-gradient centrifugation of serum from a healthy volunteer. To induce proliferation of T-LAK cells, PBMCs were cultured for 48 h at a density of 1×10^6 cells/ml in a medium supplemented with 100 IU/ml recombinant human IL-2 (kindly supplied by Shionogi Pharmaceutical Co., Osaka, Japan) in a culture flask (A/S Nunc, Roskilde, Denmark) precoated with OKT3 mAb (10 μg/ml). Proliferated cells then were transferred to another flask and expanded for 2 to 3 weeks in a culture medium containing 100 IU/ml IL-2, as reported previously (Kodama *et al.*, 2002).

Flow cytometric analyses

Test cells (1×10^6) were incubated on ice with 200 pmol of BsAb for 30 min. The incubated cells were washed with PBS containing 0.1% NaN_3 and then exposed for 30 min on ice to fluorescein isothiocyanate (FITC)–conjugated secondary antibody with affinity for c-myc tag (9E10, Santa Cruz Biotechnology, Santa Cruz, CA, USA). The stained cells were analyzed by flow cytometry (FACSCalibur, Becton Dickinson, San Jose, CA, USA) (Asano *et al.*, 2006).

In vitro growth inhibition assay

In vitro growth inhibition of TFK-1 cells (a human bile duct carcinoma line) was assayed with a 3-(4,5-dimethylthiazole-2-yl)-5-(3-carboxymethoxyphenyl)-2-(4-sulfophenyl)-2*H*-tetrazolium inner salt (MTS) assay kit (CellTiter 96 AQueous Non-Radioactive Cell Proliferation Assay; Promega, Madison, WI, USA). The target cells (5000 cells in 100 μl of culture medium) were plated in 96-well, half-well-area (A/2), flat-bottomed plates (Costar, Cambridge, MA, USA), and the plated cells were cultured overnight to allow them to adhere to the well. After removal of the culture medium by aspiration, 100 μl of T-LAK cells (effector cells) containing BsAbs at various concentrations was added to each well, giving a final effector-to-target (E:T) ratio of 5:1. After incubation of the cells for 48 h at 37°C, each well was washed with PBS three times to remove effector cells and dead target cells, and then 95 μl of culture medium containing 5 μl of a fresh mixture of MTS–phenazine methosulfate solution (Promega) was added to each well. The plates were incubated for 1 h at 37°C and then read on a microplate reader (model 3550; Bio-Rad, Hercules, CA, USA) at a wavelength of 490 nm. Growth inhibition of target cells was calculated according to the following equation: percentage growth inhibition of target cells=$[1-(A_{490}$ of experiment$-A_{490}$ of background$)/(A_{490}$ of control$-A_{490}$ of background$)] \times 100$ (Asano *et al.*, 2002a).

Isothermal titration calorimetry

Thermodynamic analyses for the interactions of hEx3 for sEGFR and CD3 were performed by microtitration calorimetry using a VP-ITC from MicroCal Inc. (Northampton, MA, USA) (Wiseman *et al.*, 1989). 1.5 μM of hEx3 in PBS (pH 7.2) containing 0.005% Tween 20 in a calorimeter cell was titrated with a 30 μM of sEGFR in the same buffer (50 μM of CD3 for 1.25 μM of hEx3). The ligand solution was injected 25 times in 10 μl portions over a period of 15 s. Data acquisition and subsequent nonlinear regression analysis were done in terms of a simple binding model, using the MicroCal ORIGIN software package.

Results

Individual preparation of each chain for hEx3 and mixtures of the chains

For refolding hEx3 diabodies from two scFv fragments, hOHh5L and h5HhOL, we applied two refolding schemes: simultaneous refolding from a mixture of unfolded hOHh5L and h5HhOL scFv fragments (refolding process I) and dimerization by mixture of refolded hOHh5L and h5HhOL fragments (refolding process II). Simultaneous refolding of hEx3 diabodies led to some aggregation of insoluble product, but more than half of the induced scFv fragments remained solubilized, and gel filtration chromatography showed that refolded scFv fragments monomorphously formed a dimeric structure [Fig. 1A and B(1)]. In the case of refolding process II, when hOHh5L and h5HhOL scFv fragments were refolded individually, the refolding ratios were approximately 20 and 10%, respectively, and gel filtration chromatography showed that hOHh5L formed both homodimers and monomers [Fig. 1B(2)], and h5HhOL formed homodimer predominantly [Fig. 1B(3)]. However, gel filtration chromatography after mixing refolded hOHh5L and h5HhOL scFv fragments showed that the mixing resulted in a single dimer fraction without monomer fractions [Fig. 1B(4)]. Each scFv fragment of hOHh5L and h5HhOL can form homodimer structures by interactions of suboptimal VH with VL, but our results imply that the interaction between cognate VH and VL regions is so strong that homodimers spontaneously converted to functional heterodimers. Table I shows the final yields of each hEx3 from two refolding methods were higher than that of secreted hEx3s in CHO cells. Although individual refolding of hOHh5L and h5HhOL scFv fragments resulted in the decrease of refolding ratio, the final amount of heterodimers prepared from insoluble aggregates in *E.coli* was larger than that of secreted antibodies from CHO cells.

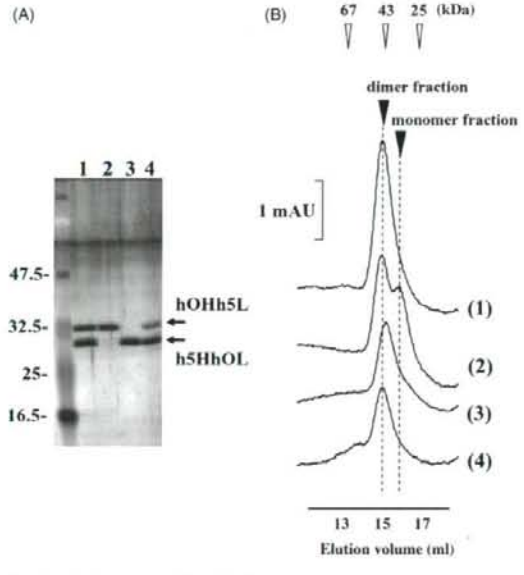

Fig. 1. (**A**) Denaturing SDS–PAGE. Molecular size markers are given on the left; the molecular weights of hOHh5L and h5HhOL were estimated to be 29 and 28 kDa, respectively. Lane 1, hEx3 from refolding process I; lane 2, refolded hOHh5L; lane 3, refolded h5HhOL; lane 4, hEx3 from refolding process II. (**B**) Gel filtration done on a Hiload Superdex 200-pg column (10/300). Elution volume is noted on the *x*-axis, and kDa are shown above the figure. (1), hEx3 from refolding process I; (2), refolded hOHh5L; (3), refolded h5HhOL; (4), hEx3 from refolding process II.

Table I. The yeld of hEx3s prepared from different methods

Prearation method	Yield (mg/l)
Refolding process I	9.6–11.2
Refolding process II	3.1–4.3
Secreted hEx3	0.7–1.3
Secreted hEx3-scDb	0.7–0.9

Refolding processes I and II for hEx3 were described in Materials and methods. Secreted hEx3s were prepared using CHO cells.

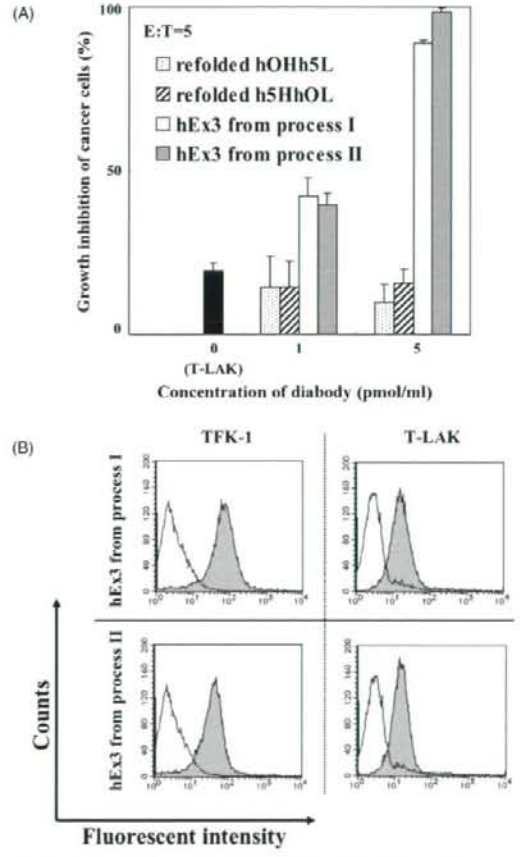

Fig. 2. (**A**) Percentage growth inhibition was determined by using a 48 h MTS assay, in which BsAb and T-LAK cells (effectors) were added to the EGFR-positive cell line TFK-1 at an effector-to-target ratio of 5:1. Data are presented as mean ± 1 SD. (**B**) Flow cytometric analysis of reactivity of constructed BsAbs with T-LAK and TFK-1 cells. Cells were incubated with PBS as a negative control (open areas). Cells were incubated with BsAb, followed by staining with FITC-conjugated anti-c-myc 9E10 antibody (gray areas).

Analysis of the biological activity of hEx3 refolded by using the two processes

We performed MTS analysis to evaluate the inhibitory effect of the generated recombinant antibodies on the growth of a human carcinoma line. Neither individually refolded hOHh5L nor h5HhOL inhibited the growth of TFK-1 (human bile duct carcinoma) cells more than T-LAK cells alone (negative control), whereas the dimers prepared by simultaneous refolding (refolding process I) or by mixing the two refolded scFv fragments (refolding process II) showed similarly intense activities (Fig. 2A). The high activity of hEx3 generated through process II also was supported by the results of a binding assay using flow cytometry: the reactivities of hEx3 from process II for CD3-positive T-LAK and EGFR-positive TFK-1 cells were similar to those of hEx3 from process I (Fig. 2B). The activation of individually refolded scFv fragments by mixing them (hEx3 from process II) indicates that the strong native interaction between appropriate VH and VL regions leads to the formation of diabodies from homodimeric and monomeric forms of the constituents.

Preparation and binding properties of secreted hEx3

To analyze the quality of the hEx3 dimer refolded from hOHh5L and h5HhOL, we co-expressed hOHh5L and h5HhOL in CHO cells and prepared hEx3 directly from culture supernatants of the transfected cells. SDS–PAGE and western blotting confirmed that hOHh5L and h5HhOL were secreted into culture supernatants in equivalent amounts (Fig. 3A), and the dimeric structure of hEx3 was confirmed by gel filtration after purification by using metal affinity chromatography

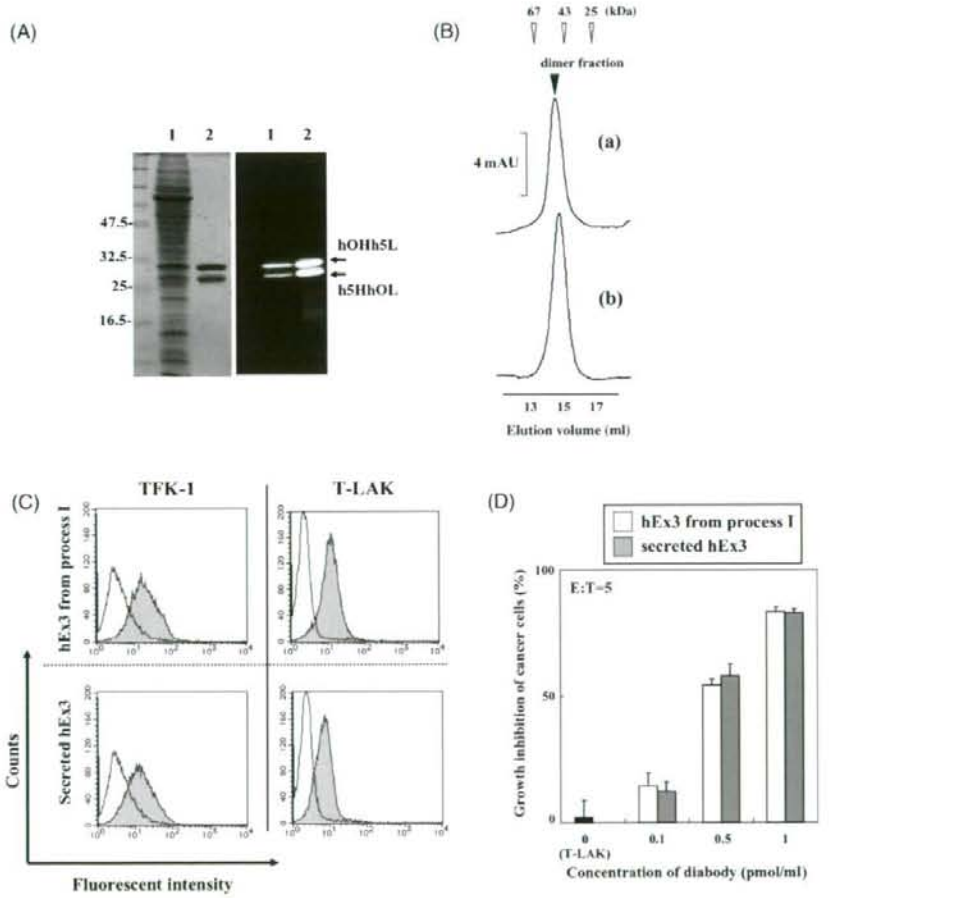

Fig. 3. (**A**) Denaturing SDS–PAGE (left) and a western blot stained with an anti-His tag monoclonal antibody (right). Lanes 1, proteins in the supernatant of CHO-expressing hEx3; Lanes 2, purified and refolded hEx3. (**B**) Gel filtration using a Hiload Superdex 200-pg column (10/300). Elution volume is noted on the *x*-axis, and kDa are shown above the figure. (a) Secreted hEx3 immediately after purification; (b) collected dimer fraction of secreted hEx3 after storage for 6 months. (**C**) Flow cytometric analysis of reactivity of constructed BsAbs with T-LAK and TFK-1 cells. Cells were incubated with PBS as a negative control (open areas). Cells were incubated with BsAb, followed by staining with an FITC-conjugated anti-c-myc 9E10 antibody (gray areas). (**D**) Percentage growth inhibition was determined by using a 48 h MTS assay, in which BsAb and T-LAK cells (effectors) were added to the EGFR-positive cell line TFK-1. The growth inhibition assay was performed at an effector-to-target ratio of 5:1. Data are presented as mean ± 1 SD.

[Fig. 3B(a)]. Flow cytometric analysis showed that the hEx3 secreted from CHO cells and the refolded hEx3 dimer from the bacterial insoluble fraction bound T-LAK and TFK-1 cells to similar extent (Fig. 3C). An MTS assay for TFK-1 using T-LAK cells at an E:T ratio of 5 also demonstrated the similarity of the dose-dependent growth inhibitory effects of the refolded and secreted hEx3 dimers (Fig. 3D). These results indicate that the hEx3 diabodies prepared by refolding from insoluble aggregates have the same quantitative activity as those secreted in the CHO expression system.

We previously used gel filtration chromatography to examine the long-term stability of the hEx3 dimer refolded from insoluble aggregates and found that the dimer remained stable for 6 months without conversion to monomers or larger aggregates (Asano *et al.*, 2006). Chromatography of CHO-expressed dimers stored for 6 months also revealed a single dimer peak [Fig. 3B(b)], indicating that the stability of the hEx3 dimer refolded from insoluble aggregates is similar to that prepared through the CHO expression system. Furthermore, the secreted hEx3 dimers retained a growth inhibition effect after 6 months (data not shown). To estimate the amount of functional heterodimer (hEx3 diabody) in the dimer fractions secreted from CHO cells, we compared their growth inhibitory effect with that of hEx3 single-chain diabodies (hEx3-scDb) secreted from CHO cells. In hEx3-scDb, hOHh5L and h5HhOL are joined by a 20-amino-acid polypeptide linker [(GGGGS)4], so that bispecific diabody conformation is achieved in the absence of homodimer byproducts (Alt *et al.*, 1999; Kipriyanov *et al.*, 1999; Korn *et al.*, 2004). In the MTS assay for TFK-1 using T-LAK cells at an E:T ratio of 5, the secreted hEx3 dimer lacking the polypeptide linker showed similar dose-dependent cancer growth inhibition to that of hEx3-scDb (Fig. 4), and thermodynamic analyses using isothermal titration calorimetry revealed stoichiometric interaction of the secreted dimer with EGFR and also with CD3 (Fig. 5; *K*a value and stoichiometry for EGFR were $2.0 \times 10^7\ M^{-1}$ and 0.9, and those for CD3 were $5.0 \times 10^6\ M^{-1}$ and 1.1). These results indicate that hEx3 dimers without polypeptide linker are secreted from CHO cells almost exclusively as functional heterodimeric diabodies. Further, given that the refolded hEx3 dimer is just as active and effective as that secreted from CHO cells, the preparation of hEx3 by refolding from insoluble hOHh5L and h5HhOL enables us to obtain a dimer fraction containing only functional bispecific diabodies.

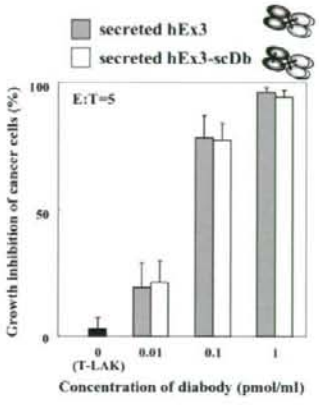

Fig. 4. Percentage growth inhibition was determined in a 48 h MTS assay, in which BsAb and T-LAK cells (effectors) were added to the EGFR-positive cell line TFK-1. The growth inhibition assay was performed at an effector-to-target ratio of 5:1. Data are presented as mean ± 1 SD.

Discussion

Recombinant BsAbs have several advantages over classic BsAbs prepared by chemical cross-linkage or the fusion of two hybridoma clones (Peipp *et al.*, 2002; Presta, 2003; Kontermann, 2005; Marvin *et al.*, 2005). The classic IgG-like BsAbs containing human Fc regions are highly effective recombinant antibodies (Carter, 2001; Marvin *et al.*, 2005;

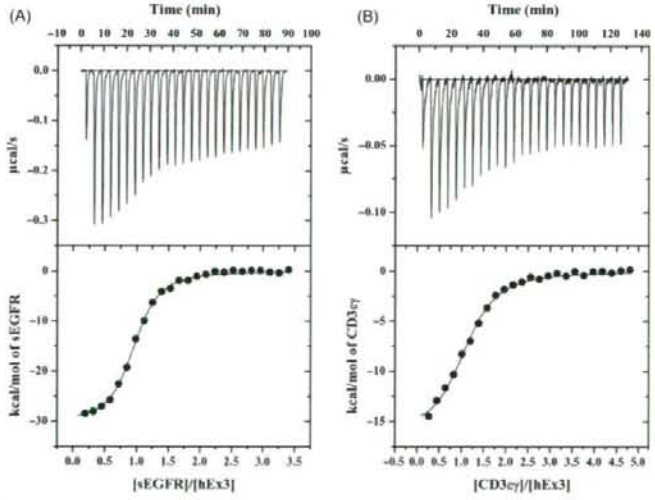

Fig. 5. Isothermal titration calorimetry of the interactions between hEx3 and sEGFR (**A**) and CD3 (**B**). Top, typical calorimetric titration at pH 7.2 and 25°C; bottom, integration plot of the data calculated from the raw data. The solid line corresponds to the best fit curve obtained by least squares deconvolution.

Asano *et al.*, 2007), but their high molecular weight leads to low yields during large-scale production. In contrast, the smaller format of bispecific diabodies affords them the advantages of rapid tissue penetration, high target retention and rapid blood clearance. Further, the decreased distance between the two antigen-binding sites of diabodies may accelerate the destruction of tumor cells by immune cells (Perisic *et al.*, 1994; Cao *et al.*, 2003; Kufer *et al.*, 2004).

We previously developed an *in vitro* refolding system to prepare functional diabodies from insoluble intracellular aggregates in *E.coli*, because bacterial systems for overexpression of diabodies often are hampered by the formation of insoluble aggregations of expressed proteins (Asano *et al.*, 2002b; Hayashi *et al.*, 2004; Asano *et al.*, 2006). The refolded bispecific diabodies showed sufficient biological activity, but refolding from two different scFv fragments leaves the possibility that the resulting dimers include inactive conformations such as homodimers. Further, contamination with homodimers remains a complication of preparing heterodimeric proteins with no covalent bonds between domains, especially recombinant antibodies constructed from VH- and VL-containing fragments, even when these proteins are prepared from soluble fractions (Zhu *et al.*, 1996; Zhu *et al.*, 1997; Fischer *et al.*, 2007). Several approaches for generating homogeneous bispecific diabodies have been attempted, including the introduction of the 'knob-into-hole' mutation into the diabody product (Zhu *et al.*, 1997). The construction of single-chain diabodies (scDb) is another alternative strategy to improve the formation of monomorphous diabodies. Bispecific scDbs are produced by connecting two scFv fragments with a polypeptide linker, so that bispecific diabodies are achieved without homodimer formation (Alt *et al.*, 1999; Kipriyanov *et al.*, 1999; Korn *et al.*, 2004).

In the present study, mixing individually refolded hOHh5L and h5HhOL scFv fragments, which each formed inactive homodimers, yielded a dimer fraction with the same activity as secreted hEx3-scDb that lacked homodimeric products (refolding process II, Figs 2A, 3D, 4 and summarized in Fig. 6). The transition between heterodimers and homodimers by domain swapping has been discussed (Kipriyanov *et al.*, 2003); the domain swapping depends on the strength of the interaction between VH and VL interfaces, that is, the weak interaction easily causes the swapping. The refolded hOHh5L scFv fragments contained a monomeric form [Fig. 1B(2)], which indicates that the improper interaction between VH domain from OKT3 Fv and VL domain from 528 Fv is weak. In contrast, strong interaction between VH and VL in humanized 528 Fv has been implied by high shape complimentary from crystallographic analysis (Makabe *et al.*, 2008). Therefore, we suggest that the strong interaction between cognate 528 VH and 528 VL domains drives the formation of homogeneous active Ex3 diabodies. Simultaneous refolding of denatured hOHh5L and h5HhOL fragments in mixture also resulted in the formation of homomorphous Ex3 diabodies, revealing that the dimers prepared by refolding from insoluble aggregates have nearly the same conformation as diabody heterodimers (refolding process I). Although there is no denying that an equilibrium of homo- and heterodimeric molecules in hEx3 solutions, the same activity of both the refolded hEx3s from refolding processes I and II as hEx3-scDb implies that the proper interaction between VH and VL domains in 528 Fv is so strong as to promote the formation of homogeneous active Ex3 diabodies. Further, the dimers secreted from CHO cells had the same

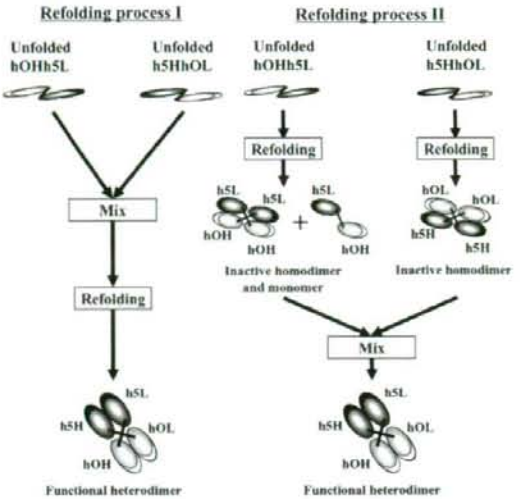

Fig. 6. Schematic diagram of results in two refolding methods for hEx3 bispecific diabody.

biological activity as hEx3-scDb (Fig. 4), and thermodynamic analyses using isothermal titration calorimetry revealed stoichiometric interaction of the secreted dimer with EGFR and also with CD3 (Fig. 5). These results demonstrate that the dimers secreted from CHO cells are equivalent to the heterodimers of hEx3 diabodies, i.e. dimer fraction of refolded hEx3 containing only functional bispecific diabodies is expected. The interdomain interaction between hOHh5L and h5HhOL in hEx3 diabodies is specific and sufficiently strong to maintain the heterodimeric structure.

In conclusion, the strong interdomain interaction between cognate VH and VL domains of hEx3 diabodies led to spontaneous formation of heterodimers, with little homodimeric contamination, through *in vitro* refolding and CHO expression. Preparation from insoluble materials using refolding is useful not only because of the high yield of recombinant proteins but also because of avoidance from influence of endogenous proteases. In fact, the yield of refolded hEx3 was approximately 10 times that of secreted hEx3 without any optimization (Table 1) and stored secreted hEx3 solution does show degradation, especially cleavage of the peptide tag (data not shown). Therefore, our *in vitro* refolding method may allow industrial-scale production of functional heterodimeric hEx3 for clinical studies. To our knowledge, this report is the first to compare the characteristics of humanized bispecific diabody prepared from insoluble material from *E.coli* with those of diabodies secreted from CHO cells.

Acknowledgement

We would like to acknowledge Shiomi Watanabe for her excellent technical assistance.

Funding

Health Sciences of the National Institute of Biomedical Innovation (07-21); Japan Society for the Promotion of Science (16106011 to I.K., 19760548 to R.A.).

References

Alt,M., Muller,R. and Kontermann,R.E. (1999) *FEBS Lett.*, **454**, 90–94.
Arndt,M.A., Krauss,J., Kipriyanov,S.M., Pfreundschuh,M. and Little,M. (1999) *Blood*, **94**, 2562–2568.
Asano,R., *et al.* (2007) *J. Biol. Chem.*, **282**, 27659–27665.
Asano,R., Kudo,T., Makabe,K., Tsumoto,K. and Kumagai,I. (2002a) *FEBS Lett.*, **528**, 70–76.
Asano,R., Kudo,T., Nishimura,Y., Makabe,K., Hayashi,H., Suzuki,M., Tsumoto,K. and Kumagai,I. (2002b) *J. Biochem. (Tokyo)*, **132**, 903–909.
Asano,R., Sone,Y., Makabe,K., Tsumoto,K., Hayashi,H., Katayose,Y., Unno,M., Kudo,T. and Kumagai,I. (2006) *Clin. Cancer Res.*, **12**, 4036–4042.
Cao,Y. and Lam,L. (2003) *Adv. Drug Deliv. Rev.*, **55**, 171–197.
Carter,P. (2001) *J. Immunol. Methods*, **248**, 7–15.
Fischer,N. and Leger,O. (2007) *Pathobiology*, **74**, 3–14.
Hayashi,H., *et al.* (2004) *Cancer Immunol. Immunother.*, **53**, 497–509.
Helfrich,W., Kroesen,B.J., Roovers,R.C., Westers,L., Molema,G. and Hoogenboom,H.R. (1998) *Int. J. Cancer*, **76**, 232–239.
Holliger,P. and Hudson,P.J. (2005) *Nat. Biotechnol.*, **23**, 1126–1136.
Kipriyanov,S.M., Moldenhauer,G., Schuhmacher,J., Cochlovius,B., Von der Lieth,C.W., Matys,E.R. and Little,M. (1999) *J. Mol. Biol.*, **293**, 41–56.
Kipriyanov,S.M., Moldenhauer,G., Braunagel,M., Reusch,U., Cochlovius,B., Le Gall,F., Kouprianova,O.A., Von der Lieth,C.W. and Little,M. (2003) *J. Mol. Biol.*, **330**, 99–111.
Kodama,H., *et al.* (2002) *Immunol. Lett.*, **81**, 99–106.
Kontermann,R.E. (2005) *Acta Pharmacol. Sin.*, **26**, 1–9.
Korn,T., Muller,R. and Kontermann,R.E. (2004) *J. Immunother.*, **27**, 99–106.
Kriangkum,J., Xu,B., Nagata,L.P., Fulton,R.E. and Suresh,M.R. (2001) *Biomol. Eng.*, **18**, 31–40.
Kufer,P., Lutterbuse,R. and Baeuerle,P.A. (2004) *Trends Biotechnol.*, **22**, 238–244.
Makabe,K., Nakanishi,T., Tsumoto,K., Tanaka,Y., Kondo,H., Umetsu,M., Sone,Y., Asano,R. and Kumagai,I. (2008) *J. Biol. Chem.*, **283**, 1156–1166.
Marvin,J.S. and Zhu,Z. (2005) *Acta Pharmacol. Sin.*, **26**, 649–658.
Peipp,M. and Valerius,T. (2002) *Biochem. Soc. Trans.*, **30**, 507–511.
Perisic,O., Webb,P.A., Holliger,P., Winter,G. and Williams,R.L. (1994) *Structure*, **2**, 1217–1226.
Presta,L. (2003) *Curr. Opin. Struct. Biol.*, **13**, 519–525.
Raso,V. and Griffin,T. (1981) *Cancer Res.*, **41**, 2073–2078.
Robinson,M.K., Doss,M., Shaller,C., Narayanan,D., Marks,J.D., Adler,L.P., Gonzalez Trotter,D.E. and Adams,G.P. (2005) *Cancer Res.*, **65**, 1471–1478.
Schlereth,B., *et al.* (2005) *Cancer Res.*, **65**, 2882–2889.
Shahied,L.S., Tang,Y., Alpaugh,R.K., Somer,R., Greenspon,D. and Weiner,L.M. (2004) *J. Biol. Chem.*, **279**, 53907–53914.
Sundaresan,G., *et al.* (2003) *J. Nucl. Med.*, **44**, 1962–1969.
Suresh,M.R., Cuello,A.C. and Milstein,C. (1986) *Methods Enzymol.*, **121**, 210–228.
Takemura,S., *et al.* (2000) *Protein Eng.*, **13**, 583–588.
Takemura,S., *et al.* (2002) *Cancer Immunol. Immunother.*, **51**, 33–44.
Tsumoto,K., Shinoki,K., Kondo,H., Uchikawa,M., Juji,T. and Kumagai,I. (1998) *J. Immunol. Methods*, **219**, 119–129.
Wiseman,T., Williston,S., Brandts,J.F. and Lin,L.N. (1989) *Anal. Biochem.*, **179**, 131–137.
Zhu,Z., Zapata,G., Shalaby,R., Snedecor,B., Chen,H. and Carter,P. (1996) *Biotechnology (NY)*, **14**, 192–196.
Zhu,Z., Presta,L.G., Zapata,G. and Carter,P. (1997) *Protein Sci.*, **6**, 781–788.

Received February 28, 2008; revised June 5, 2008; accepted June 10, 2008

Edited by Haruki Nakamura

Nanoparticles with affinity for biopolymer: Bioassisted room-temperature selective multistacking of inorganic particles on biopolymer film

Mitsuo Umetsu,[a] Takamitsu Hattori, Shinsuke Kikuchi, Itsuki Muto, Takeshi Nakanishi, Hideki Watanabe, and Izumi Kumagai[b]
Department of Biomolecular Engineering, Graduate School of Engineering, Tohoku University, Aramaki, Aoba-ku, Sendai 980-8579, Japan

(Received 1 May 2008; accepted 23 September 2008)

Recently, we selected the antibody fragment with high affinity for the biopolymer film of polyhydroxybutyrate (PHB) from human antibody fragment libraries. In this study, we functionalized CdSe quantum dot (QD) nanoparticles by orderly conjugating the anti-PHB antibody fragments to perform spontaneous and selective stacking of inorganic particles on PHB-coated plates in neutral solutions at room temperature. Surface plasmon resonance analysis showed that the orderly clustering of anti-PHB antibody fragment on QD particles led to no dissociation of QD on PHB-coated plates, indicating the availability of avidity effect. The strong spontaneous immobilization using biomolecular recognition enabled stepwise stacking of inorganic particles on PHB-coated plates only by mixing operation in neutral solutions at room temperature. We show the potential of recombinant anti-material antibody fragments for the bottom-up stacking procedures for hybrid assembly.

I. INTRODUCTION

Downsized inorganic particles can have unique electric and photonic functions, and nanoparticles are applicable for the bottom-up procedures of nanoscale devices. Appropriate patterning and stacking of nanoparticles on substrate can lead the particles to fulfill their potentials. In studies on the patterning and stacking of nanoparticles on substrates, polymer-based materials have been attractive for the development of light flexible devices in the fields of photonics,[1] electronics,[2] and sensors.[3] However, general fabrication processes involve high processing temperature, which causes some damage on polymer-based materials due to lower thermal stability of organic compounds. The techniques of patterning and stacking inorganic nanoparticles at room temperature are potentially useful for the orientation of the nanoparticles in or on heat-labile organic compounds.

Recently, several biomimetic approaches have been studied for the assembly and patterning of nano-micro materials at room temperature.[4,5] Selective adsorption of inorganic particles on patterned substrates can be controlled by modifying surface functional groups of substrates, and for surface modification of bulk materials, the utilization of biomolecules such as deoxyribonucleic acid (DNA), peptides and antibodies is becoming attractive because of their strong selective binding ability. Highly selective base-pairing interactions between complementary single-strand DNA chains have been used for pinpoint deposition of nanoparticles between electrocodes,[6] and the peptides with affinity for gold surfaces enabled the patterning of protein and nanoparticles on gold substrates using microcontact printing technology.[7,8]

Peptides that have the function of molecular recognition with high specificity have been widely utilized in the fields of medical chemistry and sensing. Appropriate configuration of amino acid residues in the binding site of peptides generates a specific binding ability for antigens. Several peptides with affinity for non-biological materials have been identified by means of a combinatorial library approach,[9] and the material-binding peptides have been expected to be utilized for bottom-up fabrication procedures in the field of bio-nanotechnology. The spontaneous binding in mild solutions at room temperature is utilized for the direct immobilization and orientation of proteins and nanomaterials on inorganic materials.[4,7,8] Considering that the bottom-up process needs no heat treatment, the utilization of the peptide with affinity for organic compound is advantageous for direct immobilization and patterning of inorganic particles in or on heat-labile organic compounds if we can identify the peptides.

Address all correspondence to these authors.
[a]e-mail: mitsuo@kuma.che.tohoku.ac.jp
[b]e-mail: kmiz@kuma.che.tohoku.ac.jp
DOI: 10.1557/JMR.2008.0401

In this study, we functionalized inorganic nanoparticles by orderly conjugating antibody fragments with affinity for the biopolymer film of polyhydroxybutyrate (PHB)[10] to perform spontaneous and selective stacking of inorganic particles on the organic-coated plate at room temperature. Antibodies also have high specific molecular recognition, but the binding affinity can be much stronger than peptides. Recently, antibodies with affinity for bulk material surfaces have been selected from human antibody libraries,[10,11] and further, material-binding functionalization of antibodies by peptide grafting was reported.[12] These results demonstrate the potential of antibodies for interface biomolecules. Here, we demonstrate that clustering high affinity anti-PHB antibody fragments on quantum dot (QD) nanoparticles enables strong and selective adsorption of QD particles on patterned PHB films due to the synergy of high affinity and avidity effect. We show the potential of recombinant anti-material antibody fragments for the bottom-up stacking of nanoparticles on heat-labile organic compounds at room temperature.

II. EXPERIMENTAL PROCEDURES

A. Construction of expression vector for anti-PHB Fv fragment with biotin acceptor peptide

The DNA sequence coding the variable heavy (VH) chain fragment with C-myc tag (EQKLISEEDLN) in the variable fragment (Fv), IgA hinge linker (SPSTPPTPSPSTPP), biotin acceptor peptide (AviTag; GGLNDIFEAQKIEWH) and poly-histidine tag (HHHHHH) in this order at the C-terminus as reported by Cloutier et al.,[13] was generated by overlap polymerase chain reaction (PCR) from pRA2FHL plasmid containing the Fv fragment of human anti-PHB monoclonal antibody PH7-3d3 as described previously.[10] The amplified sequences for the VH domain with the peptide-tags were inserted into the pRA vectors in exchange for the corresponding VH domain of wild-type PH7-3d3 using the *Nco*I-*Sac*II digestion site to express the Fv fragments with AviTag in the C-terminus side of VH.

B. Preparation of anti-PHB Fv fragment with biotinylated tag

We first transformed *E. coli* BL21 (DE3) by the plasmid of pBIRAcm encoding biotin ligase (Avidity Inc., Aurora, CO) and then transformed the same cells by the plasmid encoding anti-PHB Fv fragments with AviTag. The transformed *E. coli* cells were incubated in 2 × YT medium at 28 °C. Anti-PHB Fv with AviTag and biotin ligase were induced by adding 1 mM IPTG in the presence of 50 μM of D-biotin (Sigma, St. Louis, MO). The harvested cells were centrifuged and suspended in a Tris-HCl solution (50 mM, pH 8.0) with 200 mM NaCl. After sonication, the suspension was centrifuged at 6300 × g for 30 min. The pellet was solubilized in the 50 mM Tris-HCl solution (pH 8.0) with 6 M GdnHCl and 200 mM NaCl, and the solubilized Fv fragments were refined by means of a metal-chelate chromatography column that interacted with poly-histidine tag in VH and VL domains. The anti-PHB Fv fragments were refolded by gradual removal of GdnHCl by means of stepwise dialysis from 6 M to 0 M through 3, 2, 1, and 0.5 M, as described previously,[14] and the refolded Fv fragments were fractionated by a gel filtration chromatography (GE Healthcare, Little Chalfont, UK). The fractions of the renatured Fv with biotinylated tag were collected after the presence of biotin was confirmed in VH with western-blotting analysis using Streptavidin-Horseradish Peroxidase Conjugate (GE Healthcare).

C. Stacking of inorganic particles on PHB film via anti-PHB Fv

PHB (ICI, Inc., Slough, UK) was dissolved in chloroform at a concentration of 1.5% (w/v), and 15 μL of the solvent was spin-coated onto the gold plate (10 × 10 mm) at 4500 rpm for 1 min. The PHB-coated gold plate was heated at 210 °C for 30 s and then incubated at 110 °C for 24 h before heat release to room temperature. The annealed plate was soaked in a PBS solution with 0.1% (w/v) skim milk to suppress nonspecific binding of proteins and particles.

For stacking CdSe QD nanoparticles (the size; 30 nm, Invitrogen, Carlsbad, CA) on the PHB-coated plate, 200 nM anti-PHB Fv with biotinylated tag and 6.6 nM QD with streptavidin conjugated were mixed in 2 ml Tris-HCl solution (pH 8.0, 200 mM NaCl), and the plate was soaked in the mixture solution for 30 min [Fig. 1(a)]. The soaked plate was washed several times with 50 mM Tris-HCl solution (pH 8.0, 200 mM NaCl) to exclude non-specifically bound QD.

In an alternative stacking process, the PHB-coated plate was soaked in 2 mL Tris-HCl solution (50 mM, 200 mM NaCl, pH 8.0) containing 200 nM anti-PHB Fv with biotinylated tag for 60 min at room temperature. After the soaked plate was washed by Tris-HCl solution (50 mM, 200 mM NaCl, pH 8.0), the plate was soaked in 2 ml 6.6 nM streptavidin-conjugated QD solution (50 mM Tris-HCl, 200 mM NaCl, pH 8.0) [Fig. 1(b)]. After washing, the plate was soaked in 2 mL Tris-HCl solution (50 mM, 200 mM NaCl, pH 8.0) containing 1 μM ZnO-binding peptide (EAHVMHKVAPRP[15]) with biotin at the N-terminus via SGGG sequence, and then in 2 ml fluorescent ZnO (size; ~1 μm, Kasei Optonix, Odawara, Japan) particle suspension. Finally, the plate was excited at 365 nm after washing operation was applied again.

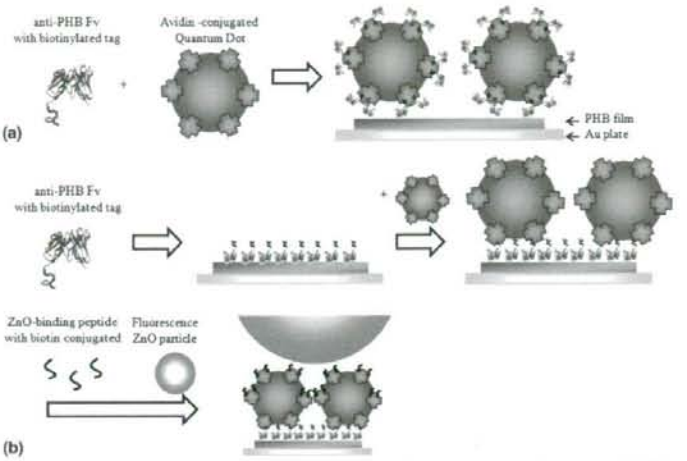

FIG. 1. Schemes for stacking inorganic particles on PHB-coated gold plate using anti-PHB Fv and ZnO-binding peptide.

D. SPR analysis

For SPR analysis, a sensor chip of Au (Biacore AB, Uppsala, Sweden) cleaned by ultraviolet-generated ozone gas, was spin-coated by PHB-chloroform solvent (0.5% w/v) at 6000 rpm. The PHB-coated plate was annealed with the same method as the gold plate for stacking experiment (see Sec. II. C). The SPR resonance angle was confirmed to be within the range needed to detect binding. SPR measurements were performed using Biacore 2000 (Biacore). The running solution for the experiments was PBS solution and it was run at the rate of 10 μl/min.

III. RESULTS

A. Selective immobilization of QD with anti-PHB Fv on PHB film

Figure 2 shows the immobilization experiment of QD particles via anti-PHB Fv. To make QD particles on which anti-PHB Fv fragments were orderly displayed, the streptavidin-conjugated QD particles were mixed with anti-PHB Fv with biotinylated tag at the C-terminus of VH. When we soaked the untreated and PHB-coated gold plates in the solution containing streptavidin-conjugated QD without antibodies, little fluorescence derived from QD was observed on both the plates [Fig. 2(a)]. In contrast, the use of the QD particles with anti-PHB Fv resulted in intense fluorescence from QD on the PHB-coated gold plate, but not on the untreated plate [Fig. 2(b)]. The Fv-displayed QD particles were specifically immobilized on PHB film. In addition, we orderly conjugated anti-lysozyme Fv fragments on QD using the same method as for anti-PHB Fv, and the immobilization of the Fv-displayed QD particles on PHB-coated plate was attempted [Fig. 2(c)]; consequently, no fluorescence derived from QD was observed on both the untreated and PHB-coated gold plates. The selective recognition ability of anti-PHB Fv enabled spontaneous immobilization of QD on PHB film.

To analyze the binding properties of the QD particles with anti-PHB Fv on PHB film, we measured the interaction of QD with PHB film via anti-PHB Fv by

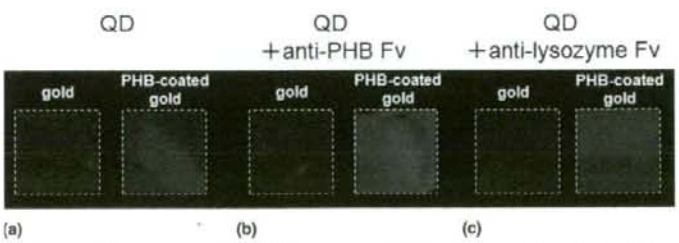

FIG. 2. Immobilization experiment of QD on untreated and PHB-coated gold plates: (a) streptavidin-conjugated QD particles, (b) streptavidin-conjugated QD particles with biotinylated anti-PHB Fv, and (c) streptavidin-conjugated QD particles with biotinylated anti-lysozyme Fv. All the plates were excited at 365 nm.

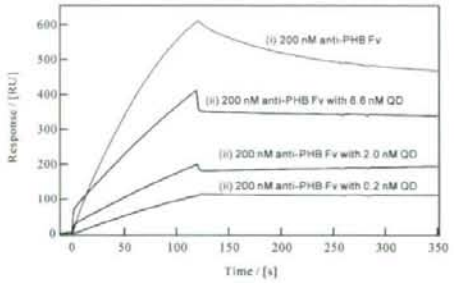

FIG. 3. SPR sensorgrams for the interaction of anti-PHB Fv with PHB-coated gold surface on sensor chip: (i) 200 nM biotinylated anti-PHB Fv solution was applied for 120 s (gray line), and (ii) 200 nM biotinylated anti-PHB Fv solutions after mixing with avidin-conjugated QD particles at concentrations of 0.2 nM, 2 nM, and 6.6 nM. QD particles were applied for 120 s (black line).

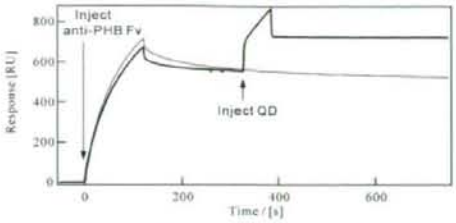

FIG. 4. SPR sensorgrams for the binding behavior of the stepwise immobilization of anti-PHB Fv and avidin-conjugated QD particles on PHB-coated gold surface on sensor chip. The 200 nM biotinylated anti-PHB Fv fragments were applied to PHB-coated gold surface, and then 0.2 nM avidin-conjugated QD particles was associated for 60 s, 320 after the start of dissociation process.

measuring SPR (Fig. 3). The binding of anti-PHB Fv with biotinylated tag to PHB film on a sensor chip was confirmed, and the binding behavior was the same as described previously (gray line in Fig. 3).[10] To reconstruct the immobilization experiment of QD via anti-PHB Fv in Fig. 2(b), the streptavidin-conjugated QD particles were injected on the PHB-coated sensor chip after the QD particles were mixed with biotinylated anti-PHB Fv (black lines in Fig. 3). The applied concentrations of QD were varied from 0.2 nM and 6.6 nM at the same Fv concentration of 200 nM; that is, the QD/Fv ratios were from 1/1000 to 1/33 (streptavidin-conjugated QD particles are considered to have about 30 binding sites for bitotin molecules). Although most anti-PHB Fv fragments were free at the QD/Fv ratio of 1/1000, the association and dissociation responses became slower than anti-PHB Fv without QD. In particular, the dissociation rates of anti-PHB Fv were drastically decreased by the conjugation with QD, indicating that few anti-PHB Fv were removed in the presence of QD. The Fv-displayed QD has much higher apparent affinity than an independent anti-PHB Fv.

B. Stacking of QD and ZnO particles on PHB film via anti-PHB Fv and ZnO-binding peptide

To examine multistacking inorganic particles on PHB film, we attempted stepwise immobilization of anti-PHB Fv and streptavidin-conjugated QD particles [Fig. 1(b)]. Figure 4 shows the SPR sensorgrams for the stepwise immobilization of anti-PHB Fv and QD. The biotinylated anti-PHB Fv was first injected, and then streptavidin-conjugated QD particles were applied to the PHB-coated sensor chip. At the injection of QD, vertical increase of SPR was observed due to bulk effect because the appearance of QD in solution caused the change of dielectric constant of solution phase; however, we confirmed the binding response of QD to the anti-PHB Fv bound on the PHB-coated sensor chip, which indicates the immobilization of QD particles via the biotin-avidin interaction. It should be noted that the dissociation of anti-PHB Fv was too slow to be observed after the QD particles were applied. The slow dissociation was also observed in the one-step immobilization of anti-PHB-Fv-displayed QD on PHB film (Fig. 3). The anti-PHB Fv fragments have the site for binding to PHB film at the opposite of the C-terminus of VH so that the biotin molecules conjugated on the AviTag peptide in the C-terminus side of anti-PHB-Fv are efficiently displayed on the surface of the sensor chip. The interactions of a streptavidin-conjugated QD particle with multiple anti-PHB Fv fragments via the biotin-avidin interactions created strong avidity effect.

The stepwise stacking of QD and ZnO particles on PHB film was performed by using anti-PHB Fv and ZnO-binding peptide (Fig. 5). At the step 2 in Fig. 5, where streptavidin-conjugated QD particles were stepwise immobilized on PHB film via biotinylated anti-PHB-Fv, the fluorescence from QD was observed on PHB film [step 2 in Fig. 5(a)]. After step 2, the QD-stacked plate was soaked in the solution containing the ZnO-binding peptides with a biotin molecule at the C-terminus and then soaked in fluorescent ZnO particle suspension (step 3 in Fig. 5); under ultraviolet irradiation, green fluorescence from ZnO was observed on the red fluorescence from QD [step 3 in Fig. 5(a)], while there was no fluorescence on PHB-coated plate without the addition of streptavidin-conjugated QD [step 3 in Fig. 5(b)]. This result indicates that ZnO particles were specifically bound to QD surface via biotin-conjugated ZnO-binding peptide.

IV. DISCUSSION

The discovery of peptide with affinity for non-biological materials, such as bulk metal, semiconductor compound, and ceramics matters, opened the way for

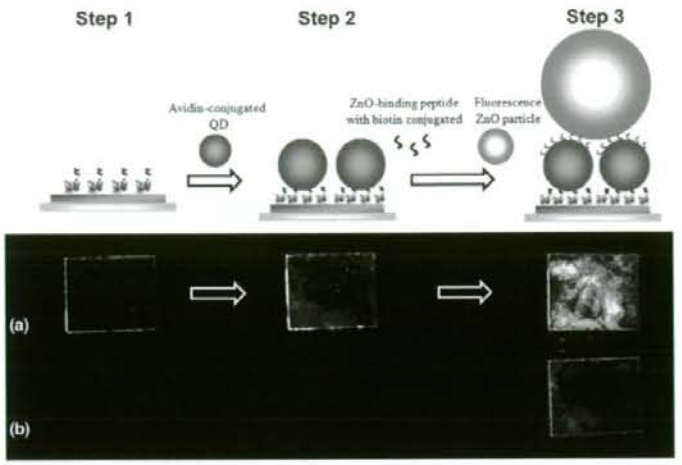

FIG. 5. Stepwise stacking of QD and ZnO particles on PHB-coated gold plate. (a) After the PHB-coated plate was soaked in 200 nM biotinylated anti-PHB Fv solution (Step 1), the plate was soaked in 6.6 nM avitin-conjugated QD solution (Step 2). After Step 2, the plate was soaked in 1 μM biotinylated ZnO-binding peptide and then in fluorescent ZnO particle suspension (Step 3). (b) After the PHB-coated plate was soaked in 200 nM biotinylated anti-PHB Fv solution (Step 1), the Step 2 process was skipped. The plate bearing anti-PHB Fv was soaked in 1 μM biotinylated ZnO-binding peptide and then in fluorescent ZnO particle suspension (Step 3). All the plates were excited at 365 nm.

utilizing the peptides as an affinity tag to enable the spontaneous and orientated immobilization of recombinant proteins on plane inorganic plates.[8] Besides the protein immobilization, recently, the patterning of gold nanoparticles via gold-binding peptide and the three-dimensional structualization by the peptides with the function of binding and mineralization have been reported.[7,15–17] A benefit of using a material-binding peptide is the application for the pattering on heat-labile substrate at room temperature. Sanghvi et al. functionalized conductive chlorine-doped polypyrrole (PPyCl) polymer using the PPyCl-binding peptide with a cell adhesive sequence at room temperature to promote cell attachment on PPyCl.[18] In this study, we applied the antibodies with affinity for the surface of organic polymer film to perform spontaneous stacking of QD particles in neutral solutions at room temperature. In the hybridization with organic and inorganic matter, the applicable conditions of temperature and solvent used are not variable in comparison with inorganic materials. The hybridization process in neutral solutions at room temperature will be potentially available for heat-labile or pH-sensitive organic compounds.

To make a strong interaction between nanoparticles and PHB films, we utilized the antibodies with high affinity for PHB film at the equilibrium dissociation constant of 14 nM.[10] The conjugation of anti-PHB Fv fragments on the surface of QD nanoparticles resulted in selective immobilization of QD on PHB film (Fig. 2). The SPR analysis implies that the anti-PHB Fv fragments conjugated on QD more strongly bind on PHB films than the Fv without QD; consequently, few anti-PHB Fv conjugated on QD were removed while running solution flowed [Fig. 3(b)]. In antibody engineering, the binding strength of antibody molecules can be promoted not only by increasing the affinity of a binding domain in an antibody, but also by increasing the number of the binding domain in an antibody. In general, the antibodies with several multiple binding domains (multivalent antibodies) generally show slow association and dissociation rates in SPR sensorgrams as the valency increases.[13,19] The change of association rate in SPR is determined by several factors, but the decrease of dissociation rate has been elucidated as avidity effect; with increased valency, the chance increases that at least one of the remaining arms will find a target before the monovalently bound complex dissociates. Therefore, the avidity effect by multidisplaying binding proteins on particles resulted in little dissociation of the Fv-conjugated QD on PHB films. Leggett et al. reported that the gold nanoparticles with multi anti-cotinine antibodies showed highly sensitive detection of the fingerprints from smokers.[20] Here, we confirmed the availability of avidity effect by orderly clustering anti-PHB antibody fragments on QD particles. Our SPR results in this study revealed clear evidence of the avidity effect by showing that the dissociation rate was drastically decreased by the use of QD. The quantitative kinetic and thermodynamic analyses are in progress.

In conclusion, we functionalized QD nanoparticles by

orderly conjugating anti-PHB antibody fragments for biopolymer PHB to perform spontaneous and selective stacking of inorganic nanoparticles on polymer-coated plate by mixing operation in neutral solutions at room temperature. SPR analysis clearly demonstrated the avidity effect causing the strong binding of the QD particles with multi antibodies. The multistacking techniques in neutral solutions at room temperature may have the potential for the bottom-up stacking procedures for hybrid assembly.

ACKNOWLEDGMENTS

This work was supported by a Scientific Research Grant from the Ministry of Education, Science, Sports, and Culture of Japan (M.U. and I.K.) and by the Industrial Technology Research Grant Program (2005) from the New Energy and Industrial Technology Development Organization (NEDO) of Japan (M.U.). This research was also partly supported by the Hosokawa foundation (M.U.).

REFERENCES

1. L. Hou, Q. Hou, Y. Mo, J. Peng, and Y. Cao: All-organic flexible polymer microcavity light-emitting diodes using 3M reflective multilayer polymer mirrors. *Appl. Phys. Lett.* **87,** 243504 (2005).
2. A.L. Briseno, S.C.B. Mannsfeld, M.M. Ling, S. Liu, R.J. Tseng, C. Reese, M.E. Roberts, Y. Yang, F. Wudl, and Z. Bao: Patterning organic single-crystal transistor arrays. *Nature* **444,** 913 (2006).
3. F. Jiang, G-B. Lee, Y-C. Tai, and C-M. Ho: A flexible micromachine-based shear-stress sensor array and its application to separation-point detection. *Sens. Actuators, A* **79,** 194 (2000).
4. S.R. Whaley, D.S. English, E.L. Hu, P.F. Barbara, and A.M. Belcher: Selection of peptides with semiconductor binding specificity for directed nanocrystal assembly. *Nature* **405,** 665 (2000).
5. C. Mao, D.J. Solis, B.D. Reiss, S.T. Kottmann, R.Y. Sweeney, A. Hayhurst, G. Georgiou, B. Iverson, and A.M. Belcher: Virus-based toolkit for the directed synthesis of magnetic and semiconducting nanowires. *Science* **303,** 213 (2004).
6. K. Keren, R.S. Berman, E. Buchstab, U. Sivan, and E. Braun: DNA-templated carbon nanotube field-effect transistor. *Science* **302,** 1380 (2003).
7. M.T. Zin, H. Ma, M. Sarikaya, and A.K-Y. Jen: Assembly of gold nanoparticles using genetically engineered polypeptides. *Small* **1,** 698 (2005).
8. T.J. Park, S.Y. Lee, S.J. Lee, J.P. Park, K.S. Yang, K-B. Lee, S. Ko, J.B. Park, T. Kim, S.K. Kim, Y.B. Shin, B.H. Chung, S-J. Ku, D.H. Kim, and I.S. Choi: Protein nanopatterns and biosensors using gold binding polypeptide as a fusion partner. *Anal. Chem.* **78,** 7197 (2006).
9. M. Sarikaya, C. Tamerler, A.K.Y. Jen, K. Schulten, and F. Baneyx: Molecular biomimetics: Nanotechnology through biology. *Nat. Mater.* **2,** 9 (2003).
10. H. Watanabe, K. Tsumoto, S. Taguchi, K. Yamashita, Y. Doi, Y. Nishimiya, H. Kondo, M. Umetsu, and I. Kumagai: A human antibody fragment with high affinity for biodegradable polymer film. *Bioconjug. Chem.* **18,** 645 (2007).
11. A.A. Schnirman, E. Zahavi, H. Yeger, R. Rosenfeld, I. Benhar, Y. Reiter, and U. Sivan: Antibody molecules discriminate between crystalline facets of a gallium arsenide semiconductor. *Nano Lett.* **6,** 1870 (2006).
12. T. Hattori, M. Umetsu, T. Nakanishi, K. Tsumoto, S. Ohara, H. Abe, M. Naito, R. Asano, T. Adschiri, and I. Kumagai: Grafting of material-binding function into antibodies. Functionalization by peptide grafting. *Biochem. Biophys. Res. Commun.* **365,** 751 (2008).
13. S. Cloutier, S. Couty, A. Terskikh, L. Marguerat, V. Crivelli, M. Pugnières, J. Mani, H. Leisinger, J. Mach, and D. Deperthes: Streptabody, a high avidity molecule made by tetramerization of in vivo biotinylated, phage display-selected scFv fragments on streptavidin. *Mol. Immunol.* **37,** 17 (2000).
14. M. Umetsu, K. Tsumoto, M. Hara, K. Ashish, S. Goda, T. Adschiri, and I. Kumagai: How additives influence the refolding of immunoglobulin-folded proteins in a stepwise dialysis system. Spectroscopic evidence for highly efficient refolding of a single-chain Fv fragment. *J. Biol. Chem.* **278,** 11 (2003).
15. M. Umetsu, M. Mizuta, K. Tsumoto, S. Ohara, S. Takami, H. Watanabe, I. Kumagai, and T. Adschiri: Bioassisted room-temperature immobilization and mineralization of zinc oxide—The structural ordering of ZnO nanoparticles into a flower-type morphology. *Adv. Mater.* **17,** 21 (2005).
16. C. Tamerler, M. Duman, E. Oren, M. Gungormus, X. Xiong, T. Kacar, B. Parviz, and M. Sarikaya: Materials specificity and directed assembly of a gold-binding peptide. *Small* **2,** 1372 (2006).
17. K. Sano, S. Yoshii, I. Yamashita, and K. Shiba: In aqua structuralization of a three-dimensional configuration using biomolecules. *Nano Lett.* **7,** 10 (2007).
18. A.B. Sanghvi, K.P-H. Miller, A.M. Belcher, and C.E. Schmidt: Biomaterials functionalization using a novel peptide that selectively binds to a conducting polymer. *Nat. Mater.* **4,** 496 (2005).
19. M. Rheinnecker, C. Hardt, L.L. Ilag, P. Kufer, R. Gruber, A. Hoess, A. Lupas, C. Rottenberger, A. Plückthun, and P. Pack: Multivalent antibody fragments with high functional affinity for a tumor-associated carbohydrate antigen. *J. Immunol.* **157,** 2989 (1996).
20. R. Leggett, E. Lee-Smith, S. Jickells, and D. Russell: "Intelligent" fingerprinting: Simultaneous identification of drug metabolites and individuals by using antibody-functionalized nanoparticles. *Angew. Chem. Int. Ed. Engl.* **46,** 4100 (2007).

EUROPEAN JOURNAL OF CANCER 44 (2008) 619–626

available at www.sciencedirect.com

ScienceDirect

journal homepage: www.ejconline.com

Decreased expression of galectin-3 is associated with metastatic potential of liver fluke-associated cholangiocarcinoma

Mutita Junking[a,c], *Chaisiri Wongkham*[a,c], *Banchob Sripa*[b,c], *Kanlayanee Sawanyawisuth*[a,c], *Norie Araki*[d], *Sopit Wongkham*[a,c,*]

[a]*Department of Biochemistry, Faculty of Medicine, Khon Kaen University, 123 Mitraparb Road, Muang, Khon Kaen 40002, Thailand*
[b]*Department of Pathology, Faculty of Medicine, Khon Kaen University, Thailand*
[c]*Liver Fluke and Cholangiocarcinoma Research Center, Faculty of Medicine, Khon Kaen University, Thailand*
[d]*Department of Tumor Genetics and Biology, Graduate School of Medical Sciences, Kumamoto University, Kumamoto, Japan*

ARTICLE INFO

Article history:
Received 11 November 2007
Received in revised form
5 January 2008
Accepted 8 January 2008
Available online 12 February 2008

Keywords:
Bile duct
Cholangiocarcinoma
Galectin
Galectin-3
LGALS3
Liver fluke
Metastasis
Migration

ABSTRACT

Galectin-3, a β-galactoside-binding lectin, is a multifunctional protein implicated in a variety of biological functions, including tumour cell adhesion, proliferation, differentiation, cancer progression and metastasis. The present study was performed to clarify the impact of galectin-3 expression on patients with liver fluke-associated cholangiocarcinoma. Galectin-3 expression was examined immunohistochemically in 53 patients with intrahepatic cholangiocarcinoma, who had undergone surgery without pre-operative therapy. All bile duct epithelium expressed galectin-3 with different intensities, according to the different histological subtypes. The poorly-differentiated type expressed galectin-3 less intensely than the papillary, well- to moderately-differentiated types ($P = 0.012$). We observed the association of low galectin-3 expression with lymphatic invasion ($P = 0.002$). Suppression of galectin-3 expression in two human cholangiocarcinoma cell lines using siRNA targeted to galectin-3 significantly increased cell migration and invasion without alterations in cell proliferation. Regulation of galectin-3 expression may therefore be an alternative therapeutic approach to control metastasis of cholangiocarcinoma.

1. Introduction

Galectins are a family of carbohydrate-binding proteins that bind β-galactoside moieties with high affinity and specificity. To date, 16 members of the galectin family have been identified,[1] of which galectin-3 (Gal-3) is one of the most frequently reported on, due to its involvement in cancer progression and metastasis.[2] Gal-3 is a multifunctional protein implicated in a variety of biological functions, including tumour cell adhesion, proliferation, differentiation, angiogenesis, cancer progression and metastasis.[3]

Gal-3 is a chimeric gene product consisting of three distinct structural domains, including a short amino-terminal domain which controls its cellular targeting, a repetitive, collagen-like sequence which serves as a substrate for the metalloproteinase matrix and a carboxy-terminal domain containing a carbohydrate-binding site.[4] Thus, the pleiotropic biological functions of Gal-3 depend on its subcellular

* Corresponding author: Address: Department of Biochemistry, Faculty of Medicine, Khon Kaen University, 123 Mitraparb Road, Muang, Khon Kaen 40002, Thailand. Tel.: +66 43 348 386; fax: +66 43 348 375.
E-mail address: sopit@kku.ac.th (S. Wongkham).
0959-8049/$ - see front matter © 2008 Elsevier Ltd. All rights reserved.
doi:10.1016/j.ejca.2008.01.014

location. For example, extracellular Gal-3 has been implicated in cell migration, adhesion and cell–cell interactions,[5] whereas intracellular Gal-3 exhibits anti-apoptotic activity.[6,7] Gal-3 is also found in the nucleus as a nuclear matrix protein involved in pre-mRNA splicing[8] and it may regulate gene expression at the transcription level.[7,9]

Cholangiocarcinoma (CCA) is a malignancy of bile duct epithelia and the most common liver cancer amongst both males and females in Northeast Thailand.[10] The incidence of CCA has also been increasing in industrialised countries.[11] The established risk factors for CCA in the West include primary sclerosing cholangitis, Caroli's disease, congenital choledochal cysts and chronic intrahepatic lithiasis,[11] whereas liver fluke (*Opisthorchis viverrini*) infection is the major risk factor in Southeast Asia.[10] The strong association between the occurrence of CCA and of liver fluke infection has been demonstrated both in experimental animal[12] and in epidemiological studies.[13–15] The mechanism by which liver fluke infection contributes to the carcinogenesis of CCA is not well understood. However, the bile duct injury resulting from liver fluke inhabitation, and the immunopathologic processes due to host immune responses to that inhabitation are suspected to be the main causes of carcinogenesis in liver fluke-associated CCA.[10]

CCA is a highly invasive/metastasising malignancy that is difficult to be diagnosed until the advanced or disseminated stage, resulting in poor prognosis. A number of studies have examined the prognostic factors of CCA; however, the exact mechanism underlying the aggressiveness of this cancer has not been clarified. We recently established a serial analysis of gene expression (SAGE) of the primary and corresponding metastatic tumours from a Thai male with CCA (http://cgap.nci.nih.gov). Using a SAGE Digital Gene Expression Displayer, we found a differentially low expression of Gal-3 (LGALS3; SAGE tag: TTCACTGTGA) in the metastatic tumour versus the primary tumour. This is interesting since evidence indicates a correlation of Gal-3 expression to neoplastic progression in various cancers.[16,17]

Even though there is substantial evidence regarding Gal-3 expression in cancer, it is yet to be determined as to how Gal-3 functions in cancer. Nevertheless, some common characteristics of Gal-3-expressing cancer cells, such as uncontrolled proliferation, disturbed adhesiveness and resistance to apoptosis, have been reported. The relevance of these observations to the mechanistic role of Gal-3 in the carcinogenesis and progression of CCA has not been examined. Herein, however, we present evidence that down-regulation of Gal-3 in CCA tissue is associated with poor differentiation of cells and lymphatic invasion. In addition, we further explore the clinicopathological significance of low Gal-3 expression in CCA.

2. Materials and methods

2.1. Human CCA specimens

The 53 paraffin-embedded liver tissues from the primary tumours of intrahepatic CCA patients were obtained from the specimen bank of the Liver Fluke and Cholangiocarcinoma Research Center, Faculty of Medicine, Khon Kaen University, Thailand. Our research protocols were approved by the Human Research Ethics Committee, Khon Kaen University (#HE471214) and informed consent was obtained from each subject before surgery.

All CCA subjects were hepatectomised and the operative procedures for all patients were intended to cure. Pre-operative diagnosis and staging of CCA patients were evaluated from clinical features, chest X-ray, ultrasonography, computed tomography (CT) and magnetic resonance cholangiopancreatography (MRCP). The age, sex, tumour location, tumour size, histological grading and pTNM stage[18] were evaluated from the medical charts and pathologic records. Normal, hyper- and dys-plastic biliary epithelia were examined from non-cancerous portions of CCA liver tissues.

2.2. Immunohistochemistry

Gal-3 was detected on the formalin-fixed, paraffin-embedded sections using standard immunohistochemistry protocols. Specifically, the paraffin sections were deparaffinised, then hydrated, and the endogenous peroxidase was blocked with H_2O_2. After blocking with normal horse serum, the sections were incubated with 1:1500 mouse anti-Gal-3 (Chemicon, Temecula, CA, United States) at 4 °C overnight, followed by 1:200 goat antimouse IgG (H + L) (Zymed Laboratories, San Francisco, CA, USA). Peroxidase activity was observed using diaminobenzidine tetrahydroxychloride solution (DAB, Dako, Glostrup, Denmark) as the substrate. The sections were counterstained with haematoxylin. The positive staining was eliminated when phosphate-buffered saline was applied instead of the primary antibody. Colon tissues were used as the positive control.

The slides were evaluated independently by two investigators who had no prior knowledge of the clinicopathological and survival data. The frequency of Gal-3 positive cells was semi-quantitatively scored on the basis of the percentage of positive cells as 0% = negative; 1–25% = +1; 26–50% = +2; and >50% = +3. The intensity of Gal-3 expression was scored as weak = 1, moderate = 2 and strong = 3. The average Gal-3 expression of each section was calculated as intensity multiplied by frequency and categorised as low (≤2) or high (>2).

2.3. Cell lines and culture condition

Two respective CCA cell lines, KKU-100 and KKU-M214, were established as described by Sripa and colleagues.[19] KKU-100 was established from primary tumour of a 65-year-old Thai woman with CCA of porta-hepatis-poorly-differentiated tubular adenocarcinoma, whereas KKU-M214 was from the primary tumour of a 52-year-old Thai male with well-differentiated type-mass forming CCA. CCA cells were cultured in HAM-F12 (Life Technologies, Rockville, MD, USA) supplemented with 10% w/v foetal calf serum, 100 U/ml penicillin and 100 μg/ml streptomycin at 37 °C and 5% CO_2.

2.4. Transient knockdown of Gal-3 using siRNA

CCA cells (8×10^4 cells in 2 ml complete culture medium) were seeded into a 6-well plate for 24 h before transfection. The siRNA specific for human *Gal-3* derived from the mRNA

sequence (5'-GGTGCCTCGCATGCTGATAAC-3') of human Gal-3 (siGal-3) was obtained from JbioS Inc., Saitama, Japan. The siGal-3 was dissolved in annealing buffer, reheated to 95 °C for 1 min and then incubated for 1 h at 37 °C, following the protocol described previously.[20] Transfection of CCA cells with 100 pM siGal-3 was performed using Lipofectamine 2000 (Invitrogen, Carlsbad, CA) according to the manufacturer's instructions. As a mock control, cells were treated with (2 μg) Lipofectamine 2000 under identical conditions. After siRNA transfection, the plates were incubated at 37 °C for 24–72 h for further analysis.

2.5. Protein extraction and Western blot analysis

Total cell lysate extractions and Western blots were performed as previously described.[21] The blots were then probed with 1:10,000 anti-Gal-3 antibody (Chemicon, Temecula, CA, USA) or with 1:5000 anti-β actin antibody (Sigma–Aldrich, St. Louis, MO, USA) as an internal control. The immuno-reactive proteins were visualised by Western Lightning Chemiluminescence Reagents (PerkinElmer Ltd., Boston, MA, USA). Quantitative analysis of Gal-3/β-actin expression was performed using Gel-Pro analyser (Media Cybernetics, Silver Spring, MD, USA).

2.6. Cell proliferation assay

CCA cells (10^4 cells/100 μl) in a culture medium were seeded into a 96-well plate and incubated at 37 °C, 5% CO_2. The number of cells was determined using sulforhodamine B (SRB) assay at 24-h intervals for 3 d, as described previously.[21] Briefly, cells were fixed in 10% cold trichloroacetic acid for 1 h at 4 °C and stained with 0.4% w/v SRB in 1% v/v acetic acid for 30 min. After washing the excess dye with 1% acetic acid, the SRB stained cells were solubilised with 200 μl of 10 mM unbuffered Tris-base solution and the absorbance was measured at 540 nm.

2.7. Migration and invasion assay

Migration and invasion were determined using Transwell® (8 μm pore size, Corning Inc., NY, USA). Briefly, 4×10^4 of CCA cells or 48 h siGal-3 transfected cells in serum-free HAM-F12 medium were seeded into each of the upper chamber and aliquots of HAM-F12 supplemented with 10% w/v foetal calf serum were placed in the lower compartment of the chamber. After incubation at 37 °C for 12 h for the KKU-100 or 10 h for the KKU-M214, cells in the upper surface of the filter were scraped off using a cotton swab. Cells, which migrated to the underside of the filter, were fixed with 25% v/v methanol for 15 min and stained with 0.5% w/v crystal violet in 25% v/v methanol. The number of migrated cells was counted under a microscope by an independent investigator. Mean values of nine low-power fields (100× magnification) were determined. Assays were done in triplicate and two independent experiments were repeated.

For invasion assay, 4×10^4 CCA cells or siGal-3 transfected cells in complete medium were seeded into each of the 0.3-mg, pre-coated Matrigel-culture inserts (Becton-Dickinson, San Jose, CA, USA). The chamber was incubated at 37 °C, 5% CO_2, 20 h for the KKU-100 or 18 h for the KKU-M214. The number of invaded cells was determined in the same way as stated for the migration assay.

2.8. Statistical analysis

Statistical analyses were performed using Sigma Stat version 3.1 software (Systat Software UK Limited., London, United Kingdom). Expression of Gal-3 was assessed for association with various clinical and pathological parameters using the χ^2-test. Patient survival was calculated from the time of surgical resection to death and the survival curves were calculated according to Kaplan–Meier, with a log-rank test. Results from migration and invasion experiments are presented as means ± SD and the significance of the differences was addressed by Student's t-test. A P-value <0.05 was considered statistically significant.

3. Results

Of the 53 CCA patients studied, 74% were male, resulting in a male to female ratio of 2.8: 1. In this series, advanced (IVA and IVB) (88%) and intrahepatic mass-forming CCA (68%) predominated. The common metastatic sites of CCA patients in this study were diaphragm, omentum and gallbladder.

3.1. Immunohistochemical expression of Gal-3 in CCA

Immunohistochemical analysis, with anti-Gal-3 antibody of normal, hyper/dys-plastic and tumour tissues of bile duct epithelium of CCA patients, showed diffuse and strong cytoplasmic immuno-reactivity. Intraluminal macrophages but not hepatocytes were also positive for Gal-3 (Fig. 1A). The majority of bile duct epithelia exhibited cytoplasmic Gal-3, whereas only 14 of 53 cases (26.4%) had cytoplasmic with weak nuclear immuno-reactivity. Strong Gal-3 expression was observed in normal bile duct epithelium (Fig. 1A) and moderately- and well-differentiated malignant bile ducts (Fig. 1B and C). Significantly, lower Gal-3 expression was found in the poorly-differentiated type of CCA ($P = 0.012$) and was associated with lymphatic invasion ($P = 0.002$) (Fig. 1D, thin arrow) (Table 1). We did not find any correlation between the expression level or localisation of Gal-3 and other clinical and pathological findings, *e.g.* tumour staging, tumour size, vascular and neural invasions, level of serum liver enzymes or jaundice (total bilirubin >2 mg/dl).

Cumulative survival was compared amongst CCA patients with low and high expression of Gal-3. Patients with survival under 30 d were labelled 'peri-operative death' ($n = 2$) and excluded from the analysis. The median follow-up duration of patients in this study was 224 d. All patients died by the end of the follow-up period. The median survival time was 324 d (95% confidence interval (CI), 172–476 d) for CCA patients with low Gal-3 expression and 557 d (95% CI, 274–839 d) for those with high Gal-3 expression. However, we did not find a significant difference in the survival times of CCA patients with low and high Gal-3 expression (log-rank, $P = 0.281$) (Fig. 2). Multivariate Cox regression analysis revealed that tumour staging was an independent prognostic indicator for the overall survival of intrahepatic CCA patients after hepatectomy

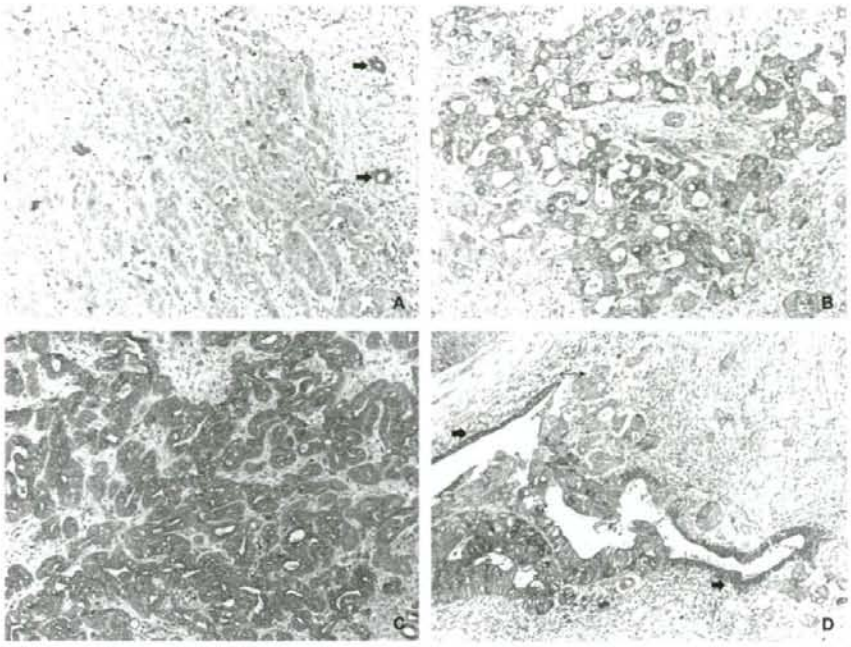

Fig. 1 – Immunohistochemistry of Gal-3 in CCA tissues. Normal bile ducts (thick arrows) and intraluminal macrophages (A), moderately- (B), and well-differentiated CCA (C) show strong expression of Gal-3. Lymphatic metastatic CCA (thin arrow) shows less Gal-3 staining compared to the normal bile ducts (thick arrow) (D). Original magnification, 100×.

(Table 2). Patients with stage IVA had better prognosis than those with stage IVB.

3.2. *Specific knockdown of Gal-3 enhances cell motility and invasion*

To address the functional importance of Gal-3, we employed RNAi to deplete the expression of Gal-3 in two CCA cell lines (viz., KKU-100 and KKU-M214). β-Actin was detected to assess the specificity of siGal-3 and the equality of protein loading in the immunoblotting analysis. The optimal level of siGal-3 (100 pM) was transfected into the cells to minimise potential off-target effects of siRNA, as shown by the expression of β-actin. As determined by Western blotting with Gal-3 antibody, cells treated with siRNA targeting 5′- GTTATCAGCATGCGAGG-CACC-3′ for 72 h significantly suppressed Gal-3 expression to 20% of the control (Fig. 3) without any observed change in the level of β-actin and cell phenotype. Mock transfection did not affect the expression level of Gal-3 or β-actin in CCA cell lines. This *in vitro* suppression of Gal-3 expression may mimic the low level of Gal-3 expression found in poorly-differentiated CCA.

siRNA knockdown of Gal-3 in CCA cells for 72 h did not affect cell proliferation as monitored by SRB assay. Mock or si-Gal-3 transfected cells exhibited similar proliferation rates (Fig. 4). No apoptotic cell-death characteristics were observed under a phase contrast microscope after either treatment. Thus, the subsequent investigations of cell migration and invasion were done within 72 h after transient knockdown with siGal-3.

The reduction of Gal-3 expression resulted in a significant increase over the parental controls in the number of cells which had migrated and invaded. The numbers of migrated cells in the siGal-3 treated groups (40 ± 11 for KKU-100 and 31 ± 9 for KKU-M214) were considerably higher than those of the controls (22 ± 5 for KKU-100, $P = 0.004$ and 19 ± 5 for KKU-M214, $P = 0.023$) (Fig. 5). A similar observation was made from the invasion assay. Significantly, more numbers of invaded cells were found in CCA cells treated with siGal-3 (142 ± 34 for KKU-100 and 135 ± 23 for KKU-M214) than the controls (21 ± 8 for KKU-100, $P < 0.001$ and 111 ± 18 for KKU-M214, $P = 0.004$) (Fig. 6).

4. Discussion

Although most galectins are ubiquitously expressed in various normal human tissues, in most cancers, galectins are either silenced or up-regulated.[22] Our data, obtained by evaluating Gal-3 expression in neoplastic bile duct epithelial tissues, show that this protein is generally expressed in normal, precancerous and malignant tumours. The intensity of Gal-3 immuno-reactivity, however, is different according to the histological grading subtype of CCA. Gal-3 was highly expressed in papillary, well- to moderately-differentiated carcinomas but down-regulated in poorly-differentiated tumours. Down-regulation of galectin-3 expression in

Table 1 – Pathological features of CCA patients and expressions of Gal-3 in primary tumour tissues

	n	Gal-3 expression		P
		Low	High	
Age				
≤56	26	9 (34.6%)	17 (65.4%)	0.471
>56	27	13 (48.1%)	14 (51.9%)	
Sex				
Male	39	15 (38.5%)	24 (61.5%)	0.663
Female	14	7 (50.0%)	7 (50.0%)	
Staging				
II–III	6	2 (33.3%)	4 (66.7%)	0.494
IVA	8	2 (25.0%)	6 (75.0%)	
IVB	39	18 (48.7%)	21 (51.3%)	
Gross type				
Intraductal growth type	13	4 (30.8%)	9 (69.2%)	0.104
Mass-forming type	36	18 (50.0%)	18 (50.0%)	
Mixed type	4	0 (0%)	4 (100%)	
Histological grading				
Invasive papillary	13	4 (30.8%)	9 (69.2%)	0.012
Well- to moderately-differentiated	25	7 (28.0%)	18 (72.0%)	
Poorly-differentiated	9	8 (88.9%)	1 (1.1%)	
Mixed	6	3(50.0%)	3 (50.0%)	
Vascular invasion				
No	20	10 (50.0%)	10 (50.0%)	0.491
Yes	33	12 (36.4%)	21 (63.6%)	
Neural invasion				
No	32	13 (40.6%)	19 (59.4%)	0.902
Yes	21	9 (42.8%)	12 (57.2%)	
Lymphatic invasion				
No	13	0 (0%)	13 (100%)	0.002
Yes	40	22 (55.0%)	18 (45.0%)	

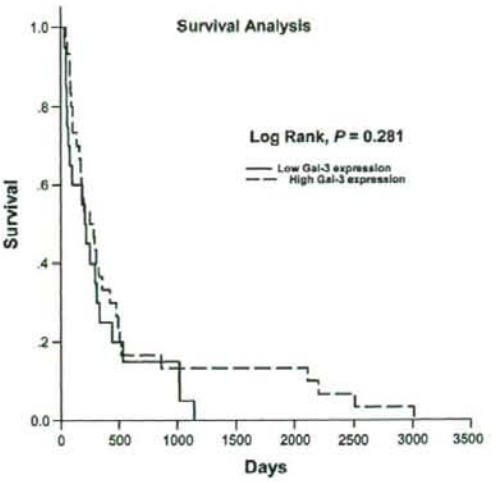

Fig. 2 – Survival curves using Kaplan–Meier method. Survival curves showed that patients with high Gal-3 expression have no significant different survival compared to those who had low Gal-3 expression ($P = 0.281$).

poorly-differentiated CCA seems to be a common phenotype of this CCA subtype since similar observation was also reported for intrahepatic CCA of Japanese patients who had no history of liver fluke infection.[23] In the present study, associations of low Gal-3 expression with poorly-differentiated CCA and lymphatic invasion were observed. These observations implied that low Gal-3 expression may correlate with unfavourable outcome since these two parameters are known to result in a poor prognosis for CCA patients.[24,25] However, the correlation of Gal-3 expression and patients' survival could not be demonstrated in the present study. This is probably due to the small number of CCA patients with low Gal-3 expression and/or with poorly-differentiated type CCA. In addition, the majority of the patients (88%) in the present study were in advanced stage with metastasis. Nevertheless, down-regulation of Gal-3 in more aggressive phenotypes has been described for CCA[23] and several human cancers, *e.g.* breast,[4] colon,[26] ovarian[27] and thyroid[28] carcinomas.

Many reports indicate multiple roles for Gal-3 in cancer pathogenesis, proliferation and metastasis; however, altering Gal-3 expression can result in increased or decreased proliferation, differentiation and metastasis in a specific way, depending on the properties of the particular cell type. The finding that down-regulation of Gal-3 expression is associated with a more aggressive type of CCA and positive lymphatic invasion prompted us to investigate the effects of Gal-3 suppression on cell growth and metastasis of CCA cell lines. Since RNA interference allows in-depth study of the molecular mechanisms of a specific gene target, we used siRNA duplexes to specifically examine the roles of Gal-3 in growth, migration and invasion of CCA cell lines *in vitro*. Our results did not support the association of Gal-3 expression and cell growth as depletion of Gal-3 by siRNA had no effect on the proliferation of the CCA cell lines studied. siRNA silencing of Gal-3 expression, however, significantly enhanced cell migration and invasion of CCA cells; thus, suppression of Gal-3 may be critical for migration and invasion of CCA.

Gal-3 functions differ depending on the site of its localisation and cell types. Expression of Gal-3 in breast carcinoma cell lines leads to rapid spread of the cells.[29] In prostate and several other cancers, however, cytosolic accumulation of Gal-3 promoted metastasis, angiogenesis and abolition of anchorage dependence, while its nuclear localisation inhibited metastasis and anchorage independence and promoted apoptosis.[26,30,31] In our study, Gal-3 was mostly found in cytoplasmic compartments of CCA tissues and can possibly be implicated in increasing cell motility and invasion. This finding is in agreement with studies on prostate cancer in which cytoplasmic Gal-3 induced significantly increased Matrigel invasion, anchorage-independent growth and *in vivo* tumour growth and angiogenesis.[30]

The role of Gal-3 in cell migration and invasion may be attributed to the cytoplasmic and extracellular Gal-3. Gal-3 can bind some cytokeratins bearing a terminal α1,3 linked *N*-acetylgalactosamine residue in cytoplasm and may modulate cell motility.[32] On the other hand, extracellular Gal-3 may exhibit numerous autocrines and paracrines which affect and mediate CCA phenotypes and functions by means of cell–cell

Table 2 – Multivariate analysis by a Cox Proportional Hazards Regression model

Variable	HR (hazard ratio)	95% confidence interval (CI)	P
Sex			
Female	1		
Male	1.155	0.57–2.31	0.685
Age			
>56	1		
<56	0.973	0.42–2.25	0.949
Gal-3 expression			
Low	1		
High	1.054	0.45–2.46	0.901
Gross type			
Intraductal growth type	1		
Mass forming	1.16	0.85–4.61	0.450
Mixed	1.26	0.33–4.85	0.726
Histological grading			
Invasive papillary	1		
Well- to moderately-differentiated	0.649	0.11–3.59	0.620
Poorly-differentiated	0.554	0.19–1.56	0.265
Mixed	0.792	0.24–2.59	0.701
Staging			
II–III	1		
IVA	0.214	0.05–0.78	0.020
IVB	1.09	0.38–3.07	0.867
Vascular invasion			
No	1		
Yes	0.635	0.30–1.13	0.216
Neural invasion			
No	1		
Yes	0.862	0.31–2.36	0.716
Lymphatic invasion			
No	1		
Yes	0.52	0.23–1.18	0.118

and cell–matrix contacts. The effect of Gal-3 as a modulator of cell adhesion is based on its multivalent properties and on its ability to bind cell surface glycoproteins and glycosylated components of the extracellular matrix. Gal-3 was shown to bind laminin, fibronectin, hensin, elastin, collagen IV and tenascin. Gal-3 also binds certain integrins ($\alpha 1\beta 1$ integrin and α subunit of $\alpha M\beta 1$ integrin), the main membrane molecules involved in cell adhesion.[33] Gal-3 can inhibit or potentiate cell adhesion of different cell types depending on its concentration. Suppression of cellular Gal-3 expression may reduce extracellular Gal-3, minimise the interaction of cell to extracellular matrix and subsequently reduce cell adhesion, which in turn would promote cell migration, as evidenced in our study. The precise mechanism(s) by which Gal-3 regulates these processes in CCA, however, needs confirmation.

Gal-3 expression depends on a complex, fine-tuned mechanism involving numerous transcription factors and signalling pathways, which varies with cell type, external stimuli and environmental conditions. The present study demonstrates the down-regulation of Gal-3 expression in poorly-differentiated and lymphatically invasive CCA. Our data, which show that the suppression of Gal-3 expression results in sig-

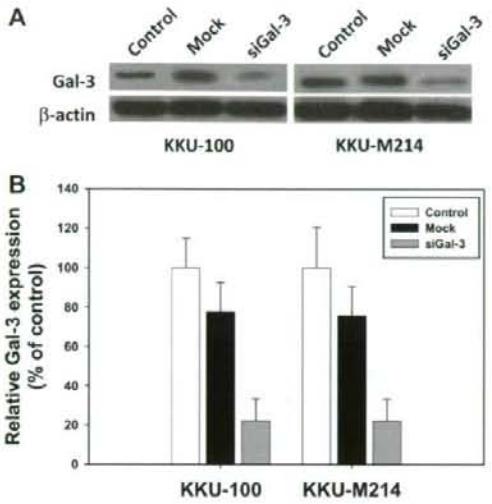

Fig. 3 – siGal-3 suppresses Gal-3 expression in CCA cell lines (viz., KKU-100 and KKU-M214). (A) Expression of Gal-3 protein by immunoblotting with anti-Gal-3. (B) Relative Gal-3 expression levels (% of parental control) after siGal-3 transfection for 72 h.

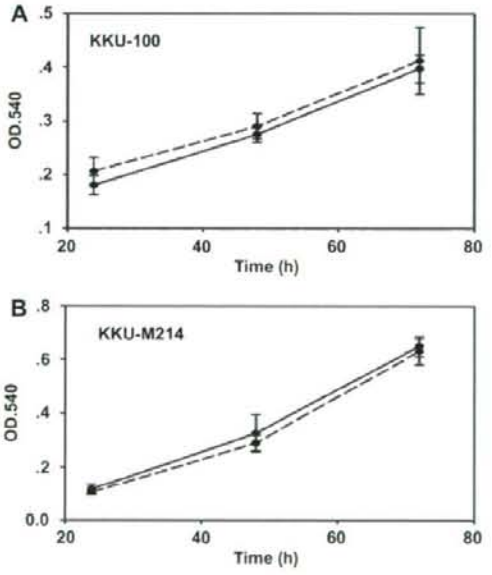

Fig. 4 – Effect of siGal-3 on cell proliferation. The number of cells was determined by SRB assay. CCA cell lines KKU-100 (A) or KKU-M214 (B) were treated with either lipofectamine (solid line) or siGal-3 (dashed line) for 24, 48 and 72 h. Each point represents averaged values from triplicates.